SERGEI ALEKSANDROVICH AKHMANOV 14 July 1929–1 July 1991

FRONTIERS IN NONLINEAR OPTICS

THE SERGEI AKHMANOV MEMORIAL VOLUME

Edited by

H WALTHER

Max-Planck-Institut für Quantenoptik, Garching

N KOROTEEV

Moscow State University, Moscow

M O SCULLY

University of New Mexico, Albuquerque

Institute of Physics Publishing
Bristol and Philadelphia

British Library Cataloguing in Publication Data
A catalogue record for this book is available from the British Library

ISBN: 0-7503-0218-6

Library of Congress Cataloging-in-Publication Data are available

Published by IOP Publishing Ltd, a company wholly owned by the Institute of Physics Publishing, London

IOP Publishing Ltd
Techno House, Redcliffe Way, Bristol BS1 6NX, England

US Editorial Office: IOP Publishing Inc, The Public Ledger Building, Suite 1035, Independence Square, Philadelphia, PA 19106

Printed in Great Britain by Galliard (Printers) Ltd, Great Yarmouth, Norfolk

ACKNOWLEDGMENT OF THE EDITORS

This volume is dedicated to the memory of our distinguished colleague Sergei Aleksandrovich Akhmanov, a pioneer in the field of nonlinear optics. The editors of this book would like to express their gratitude to all the contributors of this volume, due to their effort this book represents an in depth survey of the modern trends in nonlinear optics.

The Editors

Nonlinear generation of sub-psec pulses of THz electromagnetic radiation by optoelectronics—applications to time-domain spectroscopy

D. Grischkowsky
IBM Watson Research Center, P.O. Box 218, Yorktown Heights, NY 10598

ABSTRACT

An optoelectronic THz beam system is described, which generates and detects subpsec pulses of freely propagating THz electromagnetic radiation with a time-resolution of 150 fsec and a signal to noise ratio of more than 1000. The generated power of the THz radiation is proportional to the square of the power of the ultrafast laser driving pulses. Some applications of this system to THz time-domain spectroscopy are presented to illustrate its generality and usefulness.

INTRODUCTION

This review will first describe the optoelectronic generation and detection of freely-propagating subpsec pulses of THz electromagnetic radiation, and then it will present applications of an optoelectronic THz beam system to THz time-domain spectroscopy (TDS). Recently, there has been a great deal of work demonstrating the generation of THz radiation (1 THz = 33.3 cm^{-1} = 4.1 meV) via material and electronic excitation by ultrashort laser pulses. Modern integrated circuit techniques have made possible the precise fabrication of micron-sized dipoles, which when photoconductively driven by fsec laser pulses can radiate well into the THz regime, as shown by Auston et al (1984) and by Fattinger and Grischkowsky (1988). An alternative and complimentary approach has been to extend radio and microwave techniques into the THz regime through the use of optoelectronic antennas; Mourou et al (1981), Heidemann et al (1983), DeFonzo et al (1987a,b), Pastol et al (1988, 1990), Smith et al (1988), van Exter et al (1989, 1990) and Dykaar et al (1991). Other sources based on various physical systems and effects include the emission of an electromagnetic shock wave due to a volume dipole distribution moving faster than the phase velocity, i.e., electro-optic Cherenkov radiation discovered by Auston (1983) and developed as a free-space radiation source by Hu et al (1990). A conceptually related radiation source is the electromagnetic shock wave radiated by a surface-dipole distribution propagating faster than the phase velocity, discovered by Grischkowsky et al (1987) and demonstrated as a free-space radiation source by Fattinger and Grischkowsky (1989c). Most recently, radiation has been generated by photoconductively driving the surface field of semiconductors with ultrafast laser pulses, Zhang et al (1990). A new and quite efficient source of broadband THz radiation involves the generation of photocarriers in trap-enhanced electric fields with ultrafast laser pulses, as discovered by Katzenellenbogen and Grischkowsky (1991) and explained by Ralph and Grischkowsky (1991).

Some of these sources are based on an optical type approach whereby a transient point source of THz radiation is located at the focus of a dielectric collimating lens, followed by an additional paraboloidal focusing and collimating mirror, an arrangement introduced by Fattinger and Grischkowsky (1988, 1989a,b) and further developed by van Exter et al (1989a, 1990c). This type of source produces well collimated beams of THz radiation. Matched to an identical receiver, the resulting system has extremely high collection efficiency. With a demonstrated signal-to-noise ratio of 1000, a time resolution of less than 150 fsec and a frequency range from 0.2 THz to more than 5 THz, this optoelectronic THz system is presently the most highly developed and will be the one described in this article. One of the most useful versions of the system is based on repetitive, subpicosecond optical excitation of a Hertzian dipole antenna imbedded in a charged coplanar transmission line structure, first demonstrated by Fattinger and Grischkowsky (1988, 1989a,b) and further developed and characterized by van Exter et al (1989a, 1990c). The burst of radiation emitted by the resulting transient dipole is collimated by a THz optical system into a diffraction limited beam and focused onto a similar receiver structure, where it induces a transient voltage and is detected. The THz optical system gives exceptionally tight coupling between the transmitter and receiver, while the excellent focusing properties preserves the sub-picosecond time dependence of the source.

The combination of THz optics with the synchronously-gated, optoelectronic detection process has exceptional sensitivity for repetitively pulsed beams of THz radiation. Via two stages of collimation a THz beam with a frequency independent divergence is obtained from the THz transmitter. The THz receiver with identical optical properties collects essentially all of this beam. The resulting tightly coupled system of the THz transmitter

and receiver gives strong reception of the transmitted pulses of THz radiation after many meters of propagation. Another reason for the exceptional sensitivity is that the THz receiver is gated. The gating window of approximately 0.6 psec is determined by the laser pulsewidth and the carrier lifetime in ion-implanted silicon-on-sapphire SOS. Thus, the noise in the comparatively long time interval (10 nsec) between the repetitive THz pulses is not seen by the receiver. A final important feature of the detection method is that it is a coherent process; the electric field of a repetitive pulse of THz radiation is directly measured. Because a repetitive signal is synchronously detected, the total charge (current) from the signal increases linearly with the number of sampling pulses, while the charge (current) from noise increases only as the square root of the number of pulses.

The powerful technique of time-domain spectroscopy (TDS) has recently been applied to several different systems using a variety of sources, as described and reviewed by Grischkowsky et al (1990). With this technique two electromagnetic pulseshapes are measured, the input pulse and the propagated pulse, which has changed shape due to its passage through the sample under study. Consequently, via Fourier analyses of the input and propagated pulses, the frequency dependent absorption and dispersion of the sample can be obtained. The combination of the TDS technique with THz beams has some powerful advantages compared to traditional c.w. spectroscopy. Firstly, the detection of the THz radiation is extremely sensitive. In terms of average power the sensitivity exceeds that of liquid helium cooled bolometers, by more than 1000 times. Secondly, because of the gated and coherent detection, the thermal background, which plagues traditional measurements in this frequency range, is observationally absent. Comparing time domain spectroscopy with Fourier transform spectroscopy (FTS), it should be clear that the frequency resolution of the two techniques are similar, as they are both based on a scanning delay line, where to first order the frequency resolution is determined by the reciprocal of the time scan. Although for now FTS is superior above 4 THz (133 cm^{-1}), the limited power of the radiation sources and the problems with the thermal background favor TDS below 4 THz.

Several different type measurements will be described that illustrate the generality and usefulness of THz-TDS. An early example of THz time-domain spectroscopy was the characterization of water vapor from 0.25 THz to 1.5 THz, where the cross-sections of the 9 strongest lines were measured with the best accuracy to date by van Exter et al (1989b). Later measurements by Grischkowsky et al (1990), on single crystal sapphire and silicon were motivated by the need to find the best material for the THz lenses in

contact with the emitting and detecting chips. The available published data were inadequate for this evaluation. Absorption of the THz radiation by the lens material (initially sapphire) imposed an upper limit on the bandwidth of the entire system. The use of silicon lenses, inspired by the THz-TDS measurements of unusually low absorption and dispersion, immediately increased the system bandwidth from 2 to 3 THz and gave smoother THz pulses with less ringing structure. A THz-TDS measurement of the absorption and dispersion due to carriers in device-grade, doped silicon wafers by van Exter and Grischkowsky (1990a,b), showed that the frequency-dependent properties were completely due to the carriers and not to the host crystal. From these measurements the complex conductance was characterized over the widest frequency range to date. Finally, a experimental and theoretical study of THz coherent transients by Harde et al (1991a,b) will be reviewed. Here, after the excitation of N_2O vapor by a subpsec pulse of THz radiation, the vapor emitted a coherent THz pulse train extending to as long as 1 nsec. The origin of the emitted subpsec THz pulses (commensurate echoes) was a periodic rephasing, during the free-induction decay, of the more than fifty coherently excited rotational lines with commensurate transition frequencies. From the decay and reshaping of the echoes the coherent relaxation time T_2 and the anharmonicity factor for the N_2O molecule were evaluated.

THE OPTOELECTRONIC THz BEAM SYSTEM

A. The Experimental Set-Up.

The setup used to generate and detect beams of short pulses of THz radiation is presented in Fig.1. For this example, the transmitting and receiving antennas are identical, each consisting the antenna imbedded in a coplanar transmission line, shown in Fig. 1a as introduced by van Exter et al (1989a, 1990c). The antenna is fabricated on an ion-implanted silicon-on-sapphire (SOS) wafer. The 20-μm-wide antenna structure is located in the middle of a 20-mm-long coplanar transmission line consisting of two parallel 10-μm-wide, 1-μm-thick, 5 Ω/mm, aluminum lines separated from each other by 30 μm. A colliding-pulse mode-locked (CPM) dye laser, produces 623 nm, 70 fsec pulses at a 100 MHz repetition rate in a beam with 5 mW average power. This beam is focused onto the 5-μm-wide photoconductive silicon gap between the two antenna arms. The 70 fsec laser creation of photocarriers causes subpsec changes in the conductivity of the antenna gap. When a DC bias voltage of typically 10 V is applied to the transmitting antenna, these changes in conductivity result in pulses of electrical current through the antenna, and consequently bursts of electromagnetic radiation are produced. A large fraction of this radiation is emitted into the sapphire substrate in a cone normal to the interface; the radiation pattern is presented in Fattinger and Grischkowsky (1989b). The radiation is then collected and collimated by a dielectric lens attached to the backside (sapphire side) of the SOS wafer, an arrangement introduced by Fattinger and Grischkowsky (1988, 1989a,b). For the work reported here, the dielectric lenses were made of high-resistivity (10 kΩcm) crystalline silicon with a measured absorption of less than 0.05 cm^{-1} in our frequency range. The use of silicon gave significant improvement over the sapphire lenses previously used, although the 10% mismatch in dielectric constant between the silicon lens and the sapphire wafer causes a slight reflection. The center of the truncated 9.5 mm diameter silicon sphere (lens) is 2.0 mm above the ultrafast antenna located at the focus of the lens. As shown in Fig. 1b, after collimation by the silicon lens, the beam propagates and diffracts to a paraboloidal mirror, where the THz radiation is recollimated into a highly directional beam. Although the 70 mm aperture paraboloidal mirrors have a 12 cm focal length, a 16 cm distance was used between the silicon lenses and the mirrors to optimize the response of the system at the peak of the measured spectrum. While the high frequency components of the THz pulses remain reasonably well collimated after leaving the silicon lens, the very low frequency components quickly

diffract and illuminate the entire paraboloidal mirror, which presents a solid angle of 0.15 steradians to collect radiation from the source. After recollimation by the paraboloidal mirror, beam diameters (10-70mm) proportional to the wavelength were obtained; thereafter, all of the frequencies propagated with the same 25 mrad divergence. The combination of the paraboloidal mirror and silicon lens (THz optics) and the antenna chip comprise the transmitter, the source of a

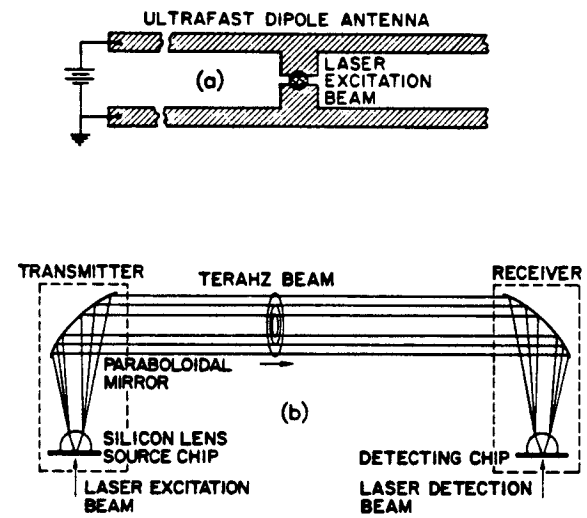

Fig.1 (a) Ultrafast dipolar antenna. (b) THz transmitter and receiver.

highly-directional freely-propagating beam of (sub)-picosecond THz pulses. After a 50 cm propagation distance this THz beam is detected by an identical combination, the THz receiver, where the paraboloidal mirror focuses the beam onto a silicon lens, which focuses it onto a SOS antenna chip, similar to the one used in the emission process. The electric field of the focused incoming THz radiation induces a transient bias voltage across the 5 μm gap between the two arms of this receiving antenna, directly connected to a low-noise current amplifier. The amplitude and time dependence of this transient voltage is obtained by measuring the collected charge (average current) versus the time delay between the THz pulses and the delayed CPM laser pulses in the 5 mW detection beam. These pulses synchronously gate the receiver, by driving the photoconductive switch defined by the 5 μm antenna gap. The

detection process with gated integration can be considered as a sub-picosecond boxcar integrator.

B. Measurements of Signal-to-Noise

A typical time-resolved measurement by van Exter and Grischkowsky (1990c) is shown in Fig.2a. The clean pulseshape is a result of the fast action of the photoconductive switch at the antenna gap, the broadband response of the ultrafast antennas, the broadband THz optical transfer function of the lenses and paraboloidal mirrors, and the very low absorption and dispersion of the silicon lenses. The measured pulsewidth of 0.54 psec (FWHM) is only

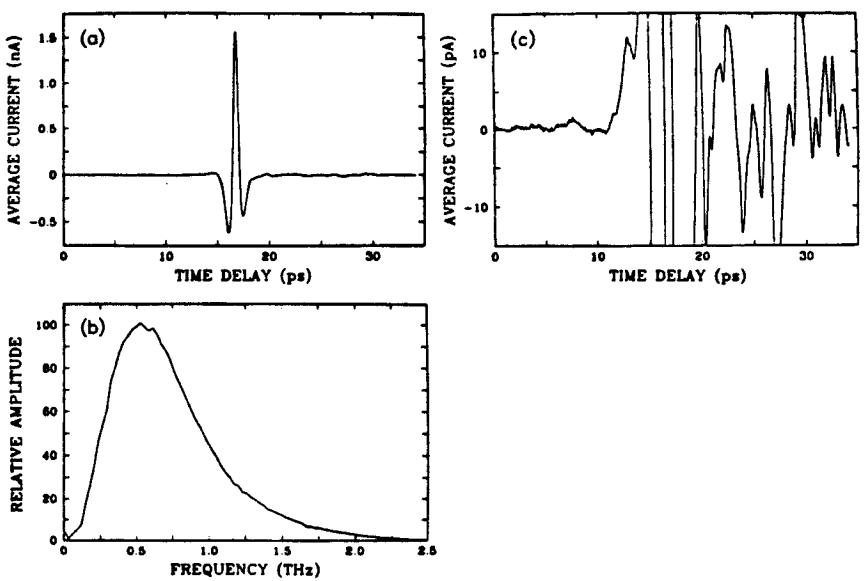

Fig.2 (a) THz pulse measured to 35 psec by scanning the time delay between the optical gating pulses and the incident THz pulses, while monitoring the current induced in the THz receiver. (b) Amplitude spectrum to 2.5 THz of the measured pulse shape. (c) THz pulse on a 100 times expanded vertical scale.

an upper limit to the true pulsewidth, because no deconvolution has been applied to the measurement to take out the response time of the antenna gap. This time-response will be determined in the next section of this article.

In Fig. 2b, the Fourier transform of the measured signal (Fig. 2a) is shown to stretch from about 0.1 to 2.0 THz. This represents only a lower limit to the true extent of the emitted radiation as it contains the frequency response of the receiver. At the low frequency end, the efficiency of both emitter and receiver has been shown to be proportional to the length of the antenna, i.e., proportional to the separation between the two lines of the coplanar transmission line. For extremely low frequencies the size of the paraboloidal mirrors will also limit the efficiency. For the high frequency limit the efficiency of the antenna is strongly reduced when 1/2 the wavelength (in the dielectric) of the emitted radiation is no longer small compared to the antenna length. This frequency for the 30 μm antenna is 1.5 Thz, so that the observed signal and corresponding spectrum is somewhat limited by the antenna response which has dropped by 50% at this frequency. The high frequency part of the spectrum is also limited by the finite risetime of the current transient and the non-ideal imaging properties of the THz optics.

In Fig. 2c, the time-resolved signal is shown on a hundred times expanded vertical scale. The structure observable after the main pulse is reproducible and is due to reflections of the electrical pulse on the transmission line, reflections of the THz pulse from the various dielectric interfaces, and absorption and dispersion of water vapor in the 1 cm path outside the vapor-tight box placed around most of the setup. The observed noise in front of the main pulse is about $1.3x10^{-13}$ A rms for an integration time of 125 ms, corresponding to an integration bandwidth of 1 Hz determined by a 12 dB/octave filter. An identical noise value is obtained when the THz beam is completely blocked. The signal-to-noise ratio in this 4 minute scan is more than 10,000:1. Another 4 minute scan is shown in Fig. 3, for which the intensity of the pump laser beam was reduced from the 6 mW normally used to only 15 μW. This 400-fold reduction in laser power led to a reduction in the transient photocurrent of 320, instead of the expected 400. The discrepancy indicates a slight nonlinearity due to the onset of saturation, related to the fact that the electrical pulses generated on the transmission line are quite strong (almost 1 V in either direction). This 320-fold reduction in photocurrent led to a reduction in the power of the THz beam by the factor $1.0x10^{-5}$. However, despite this enormous reduction in power, the peak amplitude is still more than 30 times larger than the rms noise. Based on previous calculations by van Exter and Grischkowsky (1990c) the average power in the THz beam during this measurement was about 10^{-13} W. If the

power of the THz beam were even further reduced, the detection limit of the THz receiver would be reached at $1x10^{-16}$ W, for a signal-to-noise-ratio of unity and a 125 ms integration time. Because the generation and detection of the THz (far-infrared) radiation is coherent, the THz receiver is intrinsically much more sensitive than the incoherent bolometer. The above receiver is approximately 1000 times more sensitive than a helium cooled bolometer described by Johnson et al (1980).

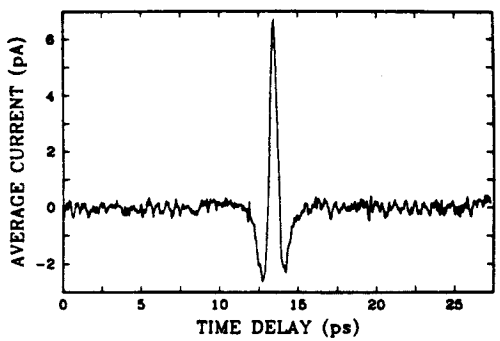

Fig.3 Measured THz pulse to 27.5 psec with a 100,000 times reduction (compared to Fig. 2a) of the THz beam power.

The THz receiver detects, with signal-to-noise ratios of approximately 10,000:1, subpsec, 14 mV pulses coming at a 100 MHz repetition rate in a highly directional beam of THz radiation with an average power of 10 nW. Consequently, the detection limit for these repetitive pulses is about 1.4 μV. However, it has been shown by van Exter and Grischkowsky (1990c) that the sampled voltage, during a single 0.6 psec gating pulse, on the receiving antenna due to the thermal background is about 0.23 mV and due to the vacuum fluctuations is 0.05 mV. Thus, in terms of instantaneous voltages, the receiver can detect 1/160 of the thermal background and 1/35 of the vacuum fluctuations. Beams of THz radiation can be detected with peak powers of only $4x10^{-5}$ that of the incident thermal radiation. This impressive performance is due to the high directionality of the THz receiver and to the fact that the thermal noise is incoherent and adds randomly for successive gating pulses, while the signal propagating in the THz beam is coherent and scales linearly with the number of gating pulses.

C. Measurements of the Time-Dependent Response Function

In this section the experimental study of the THz beam system is extended to smaller 10 μm-long antennas, which have a frequency response extending to 6 THz. From the calculated THz optical transfer function together with the known THz absorption, the limiting bandwidth of the system is extracted following the procedure of Grischkowsky and Katzenellenbogen (1991). Because the transmitter and receiver are identical, identical transmitter and receiver bandwidths are obtained. This result is compared to the calculated radiation spectrum from a Hertzian dipole driven by the current pulse determined by the laser pulsewidth, the current risetime, and the carrier lifetime. From this comparison, the time-domain response function for the antenna current is obtained.

The optoelectronic THz beam system is the same as previously described and as shown in Fig. 1, except that here smaller antennas are used.

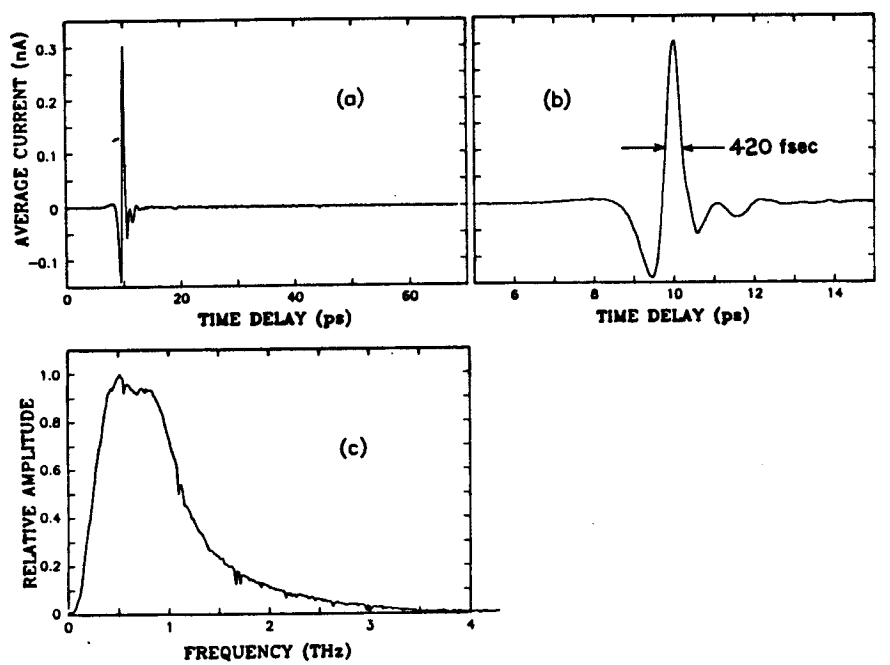

Fig.4 (a) Measured THz pulse to 70 psec. (b) Measured THz pulse on expanded 10 psec time scale. (c) Amplitude spectrum to 4 THz of Fig. 4b.

The antenna structure, again fabricated on ion-implanted SOS, is located in the middle of a 20-mm-long coplanar transmission line consisting of two parallel 5-μm-wide aluminum lines separated from each other by 10 μm. The performance of the colliding-pulse, mode-locked (CPM) dye laser was improved to provide 60 fsec excitation pulses in a beam with an average power of 7 mW on the excitation spot.

For these 10-μm-long antennas the measured transmitted THz pulse is shown in Fig. 4a. This pulse is shown on an expanded time scale in Fig. 4b, where the measured FWHM pulsewidth of 420 fsec (with no deconvolution) is indicated. This pulsewidth is significantly shorter than the 540 fsec pulse (Fig. 2a) obtained from the same experimental arrangement, but with the 30-μm-long antennas as described in the previous section. The use of even still smaller antennas did not significantly shorten the THz pulses. The numerical Fourier transform of Fig. 4a is shown in Fig. 4c, where the amplitude spectrum is seen to extend beyond 3 THz. The sharp spectral features are water lines, from the residual water vapor present in the apparatus.

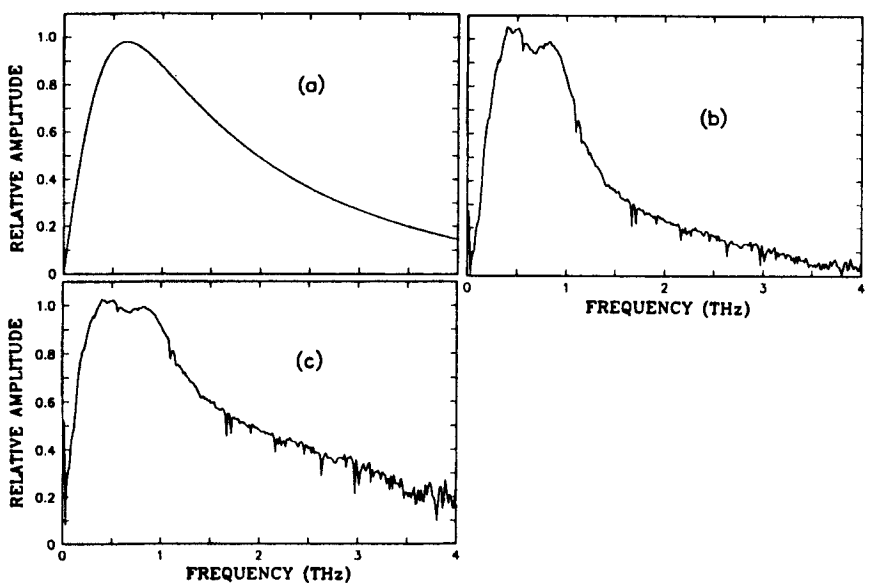

Fig.5 (a) Transmission function to 4 THz. (b) Amplitude spectrum of Fig. 4c divided by transmission function. (c) Amplitude spectral response of transmitter and receiver.

Two effects reduce the spectral extent of the measured pulse (Fig. 4c). These are the frequency-dependent transfer function, explained in detail by Lesurf (1990), of the THz optical system (Fig. 1b) and the THz absorption in the sapphire (SOS) chips The absorption of sapphire has been measured by Russell and Bell (1967), Loewenstein et al (1973) and Grischkowsky et al (1990). The transmission function describing these two effects is presented in Fig. 5a, for our focusing geometry and the SOS chip thickness of 0.46 mm. Dividing the measured spectrum in Fig. 4c by this transmission function we obtain Fig. 5b. Here, the spectral extent is determined only by the product of the receiver response and the transmitted spectrum. Because the transmitter and receiver are identical, by the reciprocity theorem explained by Monteath (1973), the transmitted spectrum is identical to the receiver response, and is given by the square root of Fig.5b shown in Fig. 5c.

D. Calculation of the Semiconductor Time-Dependent Response Function

In the small antenna limit corresponding to the Hertzian dipole, the generated radiation field is proportional to the time-derivative of the current pulse. Based on our study we conclude that the current in the antenna is mainly determined by the intrinsic response of the semiconductor itself. The intrinsic time-domain response function will now be derived for a semiconductor described by the simple Drude formalism. For this case the free carriers are considered as classical point charges subject to random collisions. Here the simplest version of this model is assumed, for which the collision damping is independent of the carrier energy and for which the frequency dependent complex conductivity $\sigma(\omega)$ is given by

$$\sigma(\omega) = \sigma_{dc} \frac{i\Gamma}{\omega + i\Gamma}, \tag{1}$$

where $\Gamma = 1/\tau$ is the damping rate and τ is the average collision time. The dc conductivity is given by $\sigma_{dc} = e\mu_{dc}N$, where e is the electron charge, μ_{dc} is the dc mobility and N is the carrier density. This relationship is in good agreement with recent time-domain spectroscopy measurements, performed by van Exter and Grischkowsky (1990a,b), on lightly doped silicon from low frequencies to beyond 2 THz. The following procedure is similar to that of Grischkowsky and Katzenellenbogen (1991). It is helpful to recast the formalism into a frequency dependent mobility as

$$\mu(\omega) = \mu_{dc} \frac{i\Gamma}{\omega + i\Gamma} . \tag{2}$$

The dc current density is given by $J_{dc} = \sigma_{dc}E$, or equivalently $J_{dc} = eE\mu_{dc}N$, where E is a constant electric field for the simple case considered here. Because of the linearity of the current in N, for a time dependent carrier density N(t), the time dependent current density can be written as

$$J(t) = eE\int_{-\infty}^{t} \mu(t - t')N(t')dt', \tag{3}$$

where μ(t-t') is the time-domain response function for the mobility. This function is determined by the inverse transform of the frequency dependent mobility to be the causal function

$$\mu(t - t') = \mu_{dc}\Gamma e^{-\Gamma(t - t')} \tag{4}$$

which vanishes for negative (t-t').

In order to facilitate the understanding of the photoconductive switch it is useful to rewrite the basic Eq. (3) in the equivalent form,

$$J(t) = eEA\int_{-\infty}^{t} \mu(t - t')\int_{-\infty}^{t'} R_c(t' - t'')I(t'')dt''dt', \tag{5}$$

where I(t'') is the normalized intensity envelope function of the laser pulse, A is a constant giving the conversion to absorbed photons/volume and R_c is the response function describing the decay of the photogenerated carriers. By defining a new photocurrent response function j_{pc}(t-t'), we can rewrite Eq.(5) in the following way

$$J(t) = \int_{-\infty}^{t} j_{pc}(t - t')I(t')dt', \tag{6}$$

where j_{pc}(t-t') is obtained by evaluating Eq.(5) with a delta function δ(t'') laser pulse. Assuming the causal function R_c(t'-t'')= exp-(t'-t'')/τ_c, describing a simple exponential decay of the carriers with the carrier lifetime τ_c (significantly longer than the average collision time τ) for positive (t'-t'') and vanishing for negative (t'-t''), and that μ(t-t') is given by the Drude response of Eq. (4), the causal response function j_{pc}(t*) is then evaluated to be

$$j_{pc}(t^*) = \frac{\mu_{dc}eEA\Gamma}{\Gamma - 1/\tau_c}(e^{-t^*/\tau_c} - e^{-t^*/\tau}) \tag{7}$$

for positive t* = (t-t') and shown to vanish for negative t*. In the short pulse limit of the ultrafast excitation pulses, the time dependence of the photocurrent J(t) is approximately equal to that of the photocurrent response function j_{pc}(t*) for positive t*. For a long carrier lifetime, the time dependence of j_{pc}(t*) is described by a simple exponential rise with a risetime of the order of $\tau = 1/\Gamma$, which is equal to 270 fsec and 150 fsec for the electrons and holes, respectively, in lightly doped silicon as measured by van Exter and Grischkowsky (1990a,b). As these results show, the material response can be slow compared to the duration of the ultrafast laser excitation pulses which can be as short as 10 fsec, but is more typically of the order of 60 fsec.

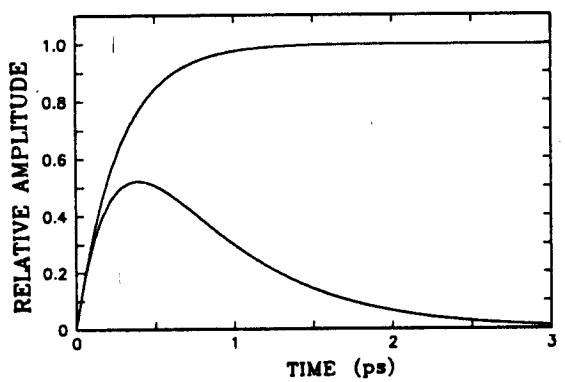

Fig.6 Calculated photoconductive response function to 3 psec with the scattering time τ = 270 fsec and infinite carrier lifetime τ_c (upper curve) and with τ_c = 600 fsec (lower curve).

The time-dependent response function described by Eq. (7) is calculated in Fig. 6 for the two cases; τ = 270 fsec and $\tau_c = \infty$, and τ = 270 fsec and τ_c = 600 fsec. The result for infinite carrier lifetime has the following intuitive interpretation. After the instantaneous creation of carriers, the initial

current and mobility is zero. The carriers then accelerate ballistically, as determined by the applied electric field, their charge and effective mass. This acceleration continues for approximately a time equal to the scattering time τ, after which the velocity and current equilibrate to their steady-state value. This discussion will now be shown to accurately describe the mathematical dependence of Eq. (7). With $\tau_c = \infty$, Eq. (7) is equal to

$$j_{pc}(t^*) = \mu_{dc} eEA(1 - e^{-t^*/\tau}), \tag{8}$$

which for times short compared to τ reduces to

$$j_{pc}(t^*) = \mu_{dc} eEAt^*/\tau. \tag{9}$$

Remembering that for Drude theory $\mu_{dc} = e/(m^*\Gamma)$, Eq. (9) is equivalent to

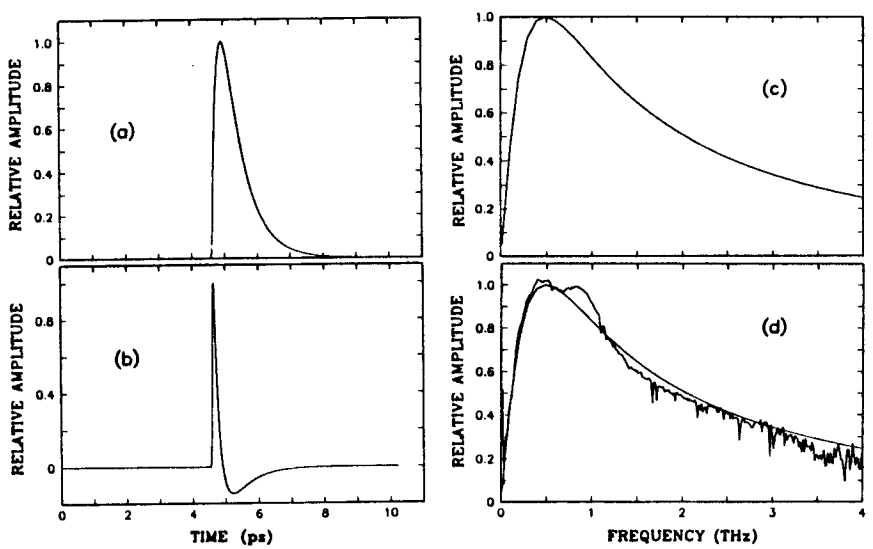

Fig.7 (a) Calculated current pulse (11 psec timescale) in semiconductor and antenna. (b) Time-derivative of current pulse. (c) Amplitude spectrum to 4 THz of Fig. 7b. (d) Comparison of Figs. 5c and 7c.

$$j_{pc}(t^*) = Aet^*(eE/m^*), \tag{10}$$

which describes the ballistic acceleration eE/m*.

For the photoconductive switches considered here, we assume the time-domain response function $j_{pc}(t^*)$ to be given by Eq. (7). This response function is then convolved with a Gaussian shaped laser pulse with a FWHM of 60 fsec, as prescribed by Eq. (6). The carrier lifetime τ_c has been measured by Doany et al (1987) to be 600 fsec for ion-implanted SOS. As demonstrated in Fig. 7, good agreement with experiment is obtained with the average collision time τ = 190 fsec. With these parameters the calculated shape of the current pulse in the photoconductive switch and the Hertzian dipole antenna is presented in Fig. 7a. The time derivative of this pulse is given in Fig. 7b, where an extremely fast transient, corresponding to the rising edge of the current pulse, is seen. The numerical Fourier transform of Fig. 7b, presented in Fig. 7c, is the predicted amplitude spectrum of the transmitter. In Fig. 7d, this spectrum is compared with the amplitude spectrum of the transmitter from Fig. 5c; the agreement is excellent. Thus, we have determined an experimentally self-consistent time-domain response function describing the current in the Hertzian dipole antenna. For longer antennas for which the radiated pulse is no longer the time-derivative of the current pulse, the calculated current pulse is Fourier analysed and the resulting spectral amplitudes are put into the antenna response to determine the emitted pulse.

In summary, we have shown that the 10-μm-long antenna imbedded in the coplanar transmission line has electrical properties much faster than the semiconductor itself. Consequently, the performance is completely determined (and limited) by the intrinsic response time of the semiconductor. With the 10-μm-long antennas, it is now possible to directly study the dynamical response of free carriers in a variety of semiconductors.

E. A High-Performance Source Utilizing Trap Enhanced Electric Fields.

A different-type, high-performance optoelectronic source chip, first used to generate pulses of freely propagating THz electromagnetic radiation by Katzenellenbogen and Grischkowsky (1991), is shown in Fig. 8d. The simple coplanar transmission line structure consists of two 10-μm-wide metal lines separated by 80 μm fabricated on high-resistivity GaAs. Irradiating the metal-semiconductor interface (edge) of the positively biased line with focused ultrafast laser pulses produces synchronous bursts of THz radiation. This occurs because each laser pulse creates a spot of photocarriers in a re-

gion of extremely high electric field, the trap enhanced field described by Ralph and Grischkowsky (1991). The consequent acceleration of the carriers generates the burst of radiation. The CPM dye laser provides 60 fsec excitation pulses with an average power of 5 mW at the 10μm diameter excitation spot. The major fraction of the laser generated burst of THz radiation is emitted into the GaAs substrate in a cone normal to the interface and is then collected and collimated by a crystalline silicon lens attached to the back side of the chip. This source chip is completely compatible with the previously described optoelectronic THz beam system .

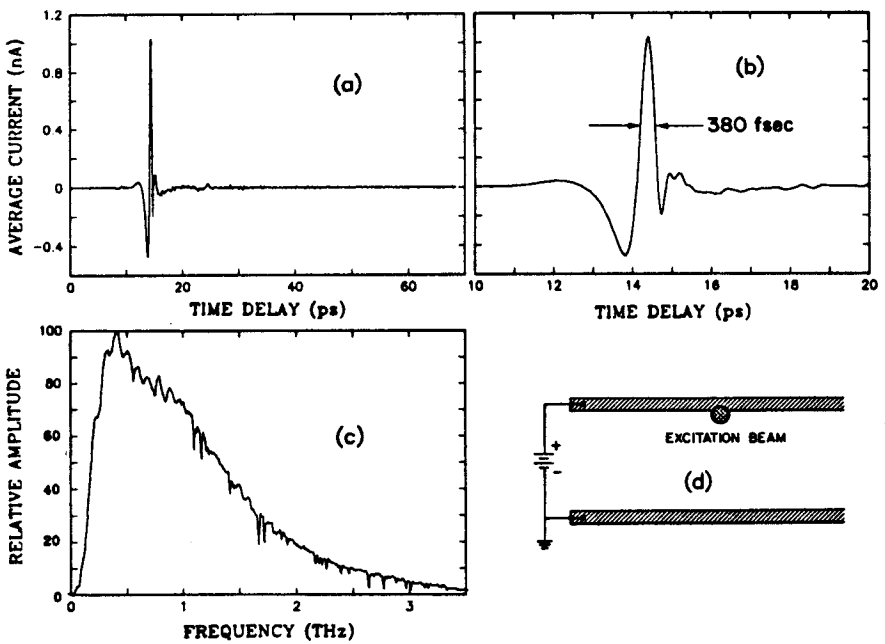

Fig.8 (a) Measured THz pulse to 70 psec. (b) Measured THz pulse on an expanded 10 psec time scale. (c) Amplitude spectrum to 3.5 THz of the THz pulse of Fig. 8a. (d) Source chip configuration used to generate the freely propagating pulses of THz radiation.

The THz radiation detector is an ion-implanted SOS detection chip with the antenna geometry shown in Fig. 1a, but with the faster 10-μm-long antenna.

The measured THz pulse emitted from the laser excited metal-GaAs interface with +60V bias across the transmission line is shown in Fig. 8a, and on an expanded time scale in Fig. 8b. The measured pulsewidth with

no deconvolution is seen to be 380 fsec. At the time these results were obtained by Katzenellenbogen and Grischkowsky (1991), they were the shortest directly measured THz pulses; the dip on the falling edge was the sharpest feature ever observed with an ion-implanted detector and indicated a response time faster than 190 fsec. The numerical Fourier transform of the pulse of Fig. 8a, as presented in Fig. 8c, extends to beyond 3 THz; the sharp line structure is due to residual water vapor present in the system.

In work (to be presented at QELS92) using this same type source and detector, but with tighter optical focusing, better matched silicon lenses and with the THz optical system of Fig. 1b optimized to have a unity, frequency-independent, transfer function, ultrashort THz pulses were measured with a ringing structure faster than 160 fsec. Their amplitude spectrum peaked at 1 THz; the relative amplitude at 3 THz was 20%, at 4 THz was 5% and useful radiation extended to 5 THz. These results confirm the response time of the receiver to be faster than 150 fsec, in agreement with the direct characterization of Grischkowsky and Katzenellenbogen (1991) and show that the entire optoelectronic system is competitive with the alternative approach of THz interferometry, Greene et al (1991) and Ralph and Grischkowsky (1992).

F. Other Sources and Receivers

As allowed by the modular nature of the THz beam system, many different combinations of antenna lengths, shapes and other semiconductors, GaAs:As, Warren et al (1990, 1991), and GaAs, Grischkowsky et al (1990), van Exter and Grischkowsky (1990b), Harde et al (1991a,b) and Warren et al (1991), have been used. For the THz source chip the carrier lifetime is of little concern, because the THz radiation is proportional to the time derivative of the current pulse and therefore, is mainly generated on the steep rising edge. Antenna of the same geometry but with longer arms between more widely separated lines produce stronger, slower pulses with lower peak frequencies as shown by van Exter and Grischkowsky (1990a,b). Different detectors can also be used. Although other materials have been tried by Warren et al (1991), ion-implanted SOS material is generally used due to its reproducible properties and short carrier lifetime. The antenna length is chosen to suit the measurement. The previously discussed 10 μm-long antenna has a relatively flat response from low frequencies to 6 THz. Slower more sensitive antennas are obtained simply by increasing the separation between the coplanar lines,

while keeping constant the 5 μm photoconductive gap separation between the two arms.

An alternative method of source characterization, which bypasses the problems of receiver bandwidth, is based on far-infrared interferometric techniques using a power detector. This approach was first demonstrated for THz radiation sources by Greene et al (1991), who measured auto-correlation signals with a fullwidth-at-half-maximum (FWHM) of 230 fsec for the THz radiation pulse from laser created carriers accelerated by the surface field of a photoconductive semiconductor. This approach used a single THz radiation source, illuminated by 10 Hz repetition-rate, amplified, 100 fsec pulses from a CPM dye laser, together with a Martin-Puplett interferometer and a liquid helium cooled bolometer. A different interferometric approach, using unamplified, 100 MHz repetition rate, CPM dye laser pulse excitation of a two source interferometer has since been demonstrated by Ralph and Grischkowsky (1992). Via this approach, together with fast, scanning-delay-line averaging, orders of magnitude improvements in the signal-to-noise ratio of the measured interferograms were obtained. Using this method, the THz radiation source of Fig. 8a was shown to produce radiation to 6 THz. In addition, a 230 fsec FWHM auto-correlation signal and an average power of 30 nW for 4 mW of laser excitation power were measured for this source.

THz TIME-DOMAIN-SPECTROSCOPY

The powerful technique of time-domain spectroscopy (TDS) has recently been applied to several different systems using a variety of sources, as described and reviewed by Grischkowsky et al (1990). With this technique two electromagnetic pulseshapes are measured, the input pulse and the propagated pulse, which has changed shape due to its passage through the sample under study. Consequently, via Fourier analyses of the input and propagated pulses, the frequency dependent absorption and dispersion of the sample can be obtained. The useful frequency range of the method is determined by the initial pulse duration and the time resolution of the detection process. Therefore, with each reduction in the generated electromagnetic pulsewidth, and/or the time resolution of detection, there is a corresponding increase in the available frequency range.

The combination of the TDS technique with THz beams has some powerful advantages compared to traditional c.w. spectroscopy. Firstly, the detection of the far-infrared radiation is extremely sensitive. Although the energy per THz pulse is very low (0.1 femtoJoule), the 100 MHz repetition rate and the coherent detection measures the electric field of the propagated pulse with a signal-to-noise ratio of about 10,000 for an integration time of 125 msec, as demonstrated by van Exter and Grischkowsky (1990c). In terms of average power this sensitivity exceeds that of liquid helium cooled bolometers, by more than 1000 times. Secondly, because of the gated and coherent detection, the thermal background, which plagues traditional measurements in this frequency range, is observationally absent. Comparing time domain spectroscopy with Fourier transform spectroscopy (FTS), it should be clear that the frequency resolution of the two techniques are similar, as they are both based on a scanning delay line, where to first order the frequency resolution is determined by the reciprocal of the time scan. However, the fact that TDS scans a delay line with a well-collimated optical beam does present some experimental advantages. Although for now FTS is superior above 4 THz (133 cm^{-1}), the limited power of the radiation sources and the problems with the thermal background favor TDS below 4 THz.

The most serious experimental problem limiting the accuracy of TDS measurements involves the relatively long term changes in the laser pulses and the consequent changes in the input THz pulses. During an experiment, we first measure the input pulse (with no sample in place), then measure the pulse transmitted through the sample, and finally remeasure the input pulse with the sample removed. This sequence is repeated several times to obtain good statistics. Typically, the amplitude spectral ratio of subsequent input

pulses varies by +/- 5% over the frequency spectrum. This variation limits the accuracy of an absorption measurement. In the same manner, the relative phase of subsequent input pulses varies by +/- 0.05 radians over the same spectrum, and thereby limits the accuracy of the measurements of the index of refraction. Another experimental consideration involves the frequency distribution across the profile of the THz beam, which consists of a series of overlapping discs with diameters proportional to the wavelength. This feature requires that the sample be uniform and be centered in the beam and that an aperture of the same diameter as the sample blocks any THz radiation from going around the sample. The aperture is kept in place for measurement of the input pulse.

We will now describe several different type measurements that illustrate the generality and usefulness of THz-TDS.

A. Water Vapor

An early example of THz time-domain spectroscopy was the characterization of water vapor from 0.25 THz to 1.5 THz, where the cross-sections of the 9 strongest lines were measured with the best accuracy to date by van Exter et al (1989b).

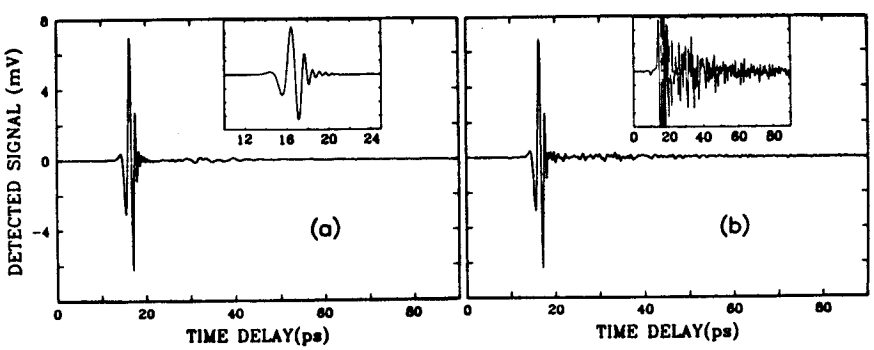

Fig.9 (a) Measured THz pulse (90 psec timescale) propagating in pure nitrogen. Inset shows pulse on an expanded 15 psec time scale. (b) Measured THz pulse with 1.5 Torr of water vapor in the enclosure. Inset shows pulse on a 20x expanded vertical scale.

For these early measurements 30 μm-long source and detector antennas on ion-implanted SOS substrates were used together with MgO lenses instead of the currently used, more optimal high-resistivity silicon. Figure 9a displays the detected THz radiation pulses after propagating through pure nitrogen. This measurement was made in a single 10 minute scan of the 200 psec relative time delay between the excitation and detection pulses. When 1.5 Torr of water vapor, corresponding to 8% humidity at 20.5° C, was added to the enclosure, the transmitted pulse changed to that shown in Fig. 9b. The additional fast oscillations are caused by the combined action of the dispersion and absorption of the water vapor lines. The slower and more erratic variations seen in both Figs. 9a and 9b result from reflections of the main pulse. They are reproducible and divide out in the data analysis. The inset shows the data on a 20X expanded vertical scale. Here, the oscillations are seen to decay approximately exponentially with an average coherent relaxation time T_2.

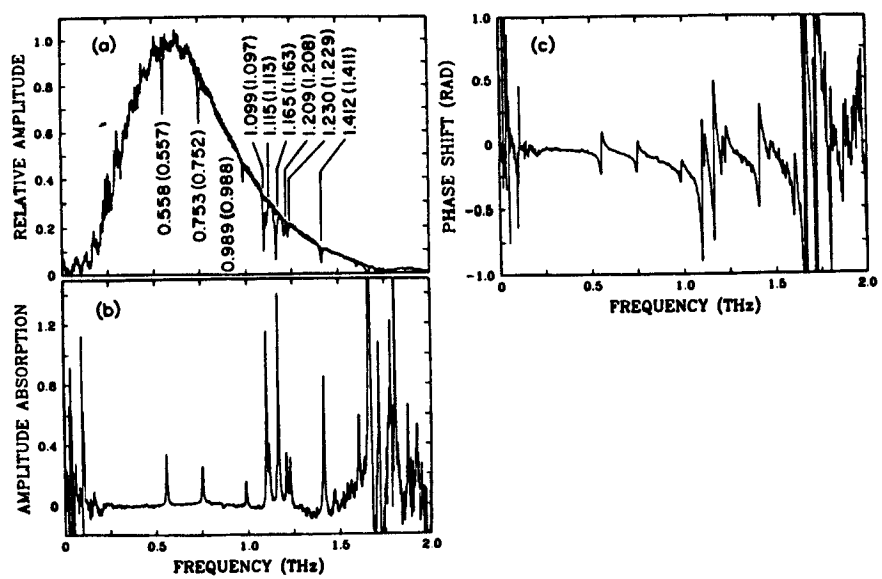

Fig.10 (a) Amplitude spectra to 2 THz of Figs. 9a and 9b. (b) Amplitude absorption coefficient obtained from Fig. 10a. (c) Relative phase of the spectral components of Fig. 10a.

The amplitude spectra of Figs. 9a and 9b are compared in Fig. 10a, where the strong water absorption lines are clearly observable. The additional structure on both spectra is not noise but results from spurious reflections of the main pulse. At each line are indicated the measured frequency with an estimated error of +/- 0.001 THz and in parenthesis the literature value. The corresponding absorption coefficients are displayed in Fig. 10b as the negative of the natural logarithm of the ratio of the two amplitude spectra in Fig. 10a. Because the electric field is directly measured, the relative phaseshift between the two spectra is also obtained as plotted in Fig. 10c, without the need of the Kramers-Kronig relations. As expected for a Lorentzian line, the magnitude of the jump in phase experienced at each resonance equals the peak absorption.

B. Sapphire and Silicon

The following measurements of Grischkowsky et al (1990) on single crystal sapphire and silicon were motivated by the need to find the best material for the THz lenses in contact with the emitting and detecting chips. The available published data were inadequate for this evaluation. Absorption of the THz radiation by the lens material (initially sapphire) imposed an upper limit on the bandwidth of the entire system.

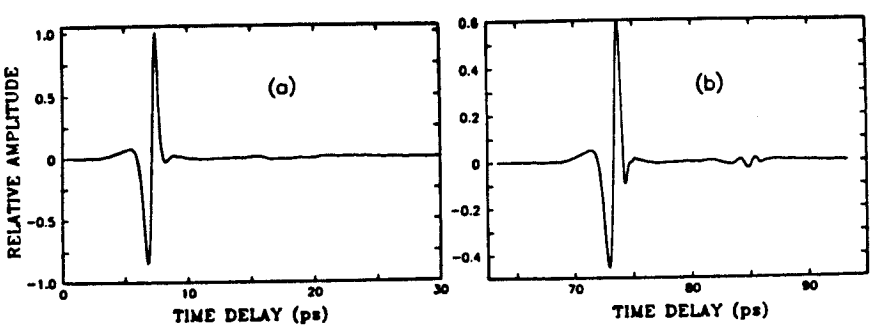

Fig.11 (a) Measured THz pulse to 30 psec. (b) Measured THz pulse (62.5-95 psec) after passage through the sapphire crystal.

The use of silicon lenses, inspired by our measurements of unusually low absorption and dispersion, immediately increased the system bandwidth from 2 to 3 THz and gave smoother THz pulses with less ringing structure.

The single crystal sapphire sample was a polished, 57 mm diameter disc, 9.589 mm thick, and with the C axis in the plane of the disc. A typical THz input pulse incident upon the sample is shown in Fig. 11a, and the output pulse (normalized to the input pulse) after propagation through the sample is shown in Fig. 11b for which the C axis of the crystal was perpendicular to the polarization. The reduction in amplitude is due to the reflective loss at both surfaces and to the absorption suffered during passage through the sapphire. The pulse at 73.4 psec delay is the ordinary pulse, while the smaller pulse at 85.1 psec delay is the extraordinary pulse. The ratio of the peak of the ordinary pulse to that of the extraordinary pulse is approximately 25:1 and gives the polarization sensitivity of our system. In terms of amplitude, the polarization ratio of the generated THz beam is 5:1. The 11.8 psec separation between the two pulses is a measure of the birefringence of sapphire and, neglecting the correction to group velocity due to dispersion, directly gives the difference in the index of refraction between the extraordinary and ordinary ray to be $n_e - n_o = 0.37$ compared to the the value of 0.34 measured by Russell and Bell (1967) and tabulated by Gray (1982). When a full frequency analysis is performed, excellent agreement is obtained with the literature value. The 73.4 psec time delay of the ordinary pulse with respect to the 7.1 psec time delay of the pulse with no sample in place gives the ordinary index of refraction $n_o = 3.07$ in agreement with the literature value. The absorption coefficient vs frequency determined from these pulses is shown in Fig. 12a. Here, we see a monotonic increase in absorption with increasing frequency with the expected quadratic dependence. Due to excessive attenuation caused by the sample being too thick for the weak higher frequency components, the data is considered to be accurate only up to 1.75 THz. Some of the previous work has been indicated on the curve, and shows a rough agreement (within a factor of 2) with the TDS measurement. The earliest work of Russell and Bell (1967) clearly gives too little absorption at low frequencies, where our results are in better agreement with those of Loewenstein et al (1973). The relative phases of the Fourier components determine the index of refraction vs frequency as presented in Fig. 12b, which compares reasonably well with the indicated earlier results.

Crystalline silicon is optically isotropic, eliminating concern about the polarization of the incident THz beam and crystal orientation. Although there is significant literature concerning the far-infrared properties of silicon, below 2 THz there are noteworthy discrepancies among the published data

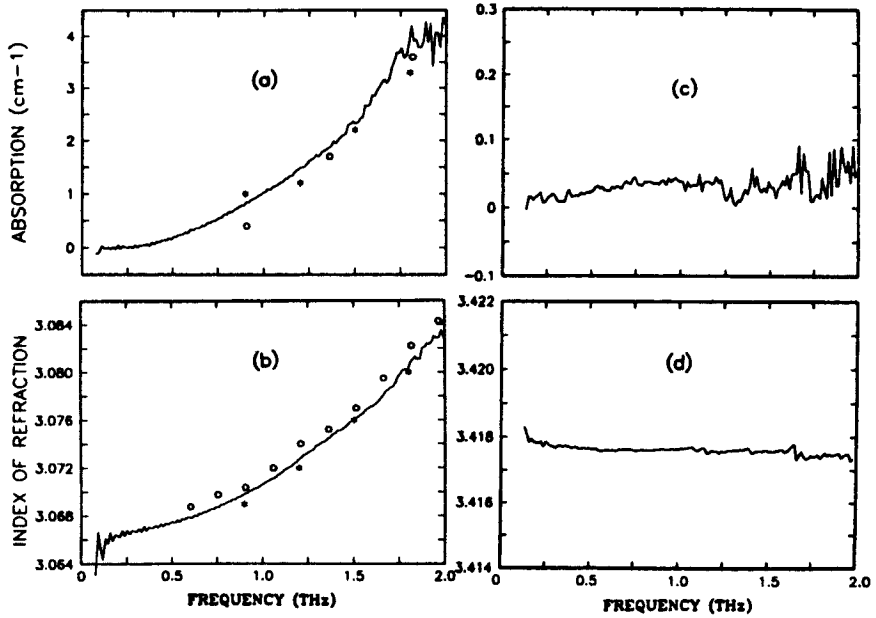

Fig.12 TDS measurements to 2 THz of crystalline sapphire and silicon. The circles are the measurements of Russell and Bell (1967) that are tabulated by Gray (1982); the asterisks are the data of Loewenstein et al (1973). (a) Ordinary ray power absorption coefficient (cm^{-1}) of sapphire. (b) Ordinary ray index of refraction of sapphire. (c) Power absorption coefficient (cm^{-1}) of high-resistivity silicon. (d) Index of refraction of high-resistivity silicon.

with variations in the measured absorption coefficients of up to 10 times. The main reason for this confusion is that below 2 THz the results are extremely sensitive to the presence of carriers. THz-TDS measurements of van Exter and Grischkowsky (1990a,b) show that for 1 Ω-cm, N-type silicon the peak absorption is 100 cm^{-1}, and that for 10 Ω-cm, N-type the absorption is 12 cm^{-1}. Extrapolating these values to 100 Ω-cm, α = 1 cm^{-1}; at 1 kΩ-cm, α = 0.1 cm^{-1}, and at 10 kΩ-cm, α = 0.01 cm^{-1}. Consequently, unless high purity, high-resistivity material is used, what is measured is not the properties of the intrinsic semiconductor but that of the carriers due to residual impurities. This problem is most prevalent in the earlier work on silicon with

resistivities of 10 Ω-cm for the sample of Russell and Bell (1967) to 100 Ω-cm for the sample of Loewenstein et al (1973).

The following TDS measurements were made on a 50 mm diameter, 20.046 mm thick single crystal of high-resistivity (greater than 10 kΩ-cm), float-zone silicon. For this material we have measured unprecedented transparency together with a remarkably flat dispersion curve. This is an excellent material for teraHz applications as can be seen from the absorption spectrum presented in Fig. 12c. Throughout the range from low frequencies up to 2 THz the measured absorption coefficient is less than 0.05 cm^{-1}. From the relative phases of the spectral components, the index of refraction vs frequency is obtained as presented in Fig. 12d. Here, the extremely desirable feature of low-dispersion is clearly evident; the index of refraction changes by less than 0.001 over the entire measured spectrum.

C. N-Type and P-Type Silicon

We now describe a THz time-domain-spectroscopy measurement by van Exter and Grischkowsky (1990a,b) of the absorption and dispersion due to carriers in device-grade, doped silicon wafers. The frequency-dependent properties were shown to be completely due to the carriers and not to the host crystal. Consequently, the complex conductance could be characterized over the widest frequency range to date. The samples used were a 283 μm thick wafer of 1.15-Ωcm, N-type and a 258 μm thick wafer of 0.92-Ωcm P-type silicon. The measured absorptions shown in Fig. 13a are more than 2000 times greater than that of the host crystal. Below 0.15 THz the data becomes noisy due to the limited beam power, but the theoretically-predicted drop in absorption at low frequencies is clearly observable. The clear difference between the N and P type material is due to the different dynamic behavior of the electrons and holes. For these measurements the oscillations due to the etalon effects of the sample geometry have been removed numerically. As shown in Fig. 13b, the index of refraction is strongly frequency dependent, having a clear minimum followed by a dramatic increase towards lower frequencies. The agreement with the Drude theory (solid line) is exceptional.

As the THz optical properties of the samples are essentially completely determined by the carrier dynamics, the complex electric conductivity of the doped silicon has also been measured. Independent of Drude theory and relying on only very general assumptions, the electric conductivity is obtained

(without any fitting parameters) from the data of Figs. 13a and 13b; the resulting real part of the conductivity is shown

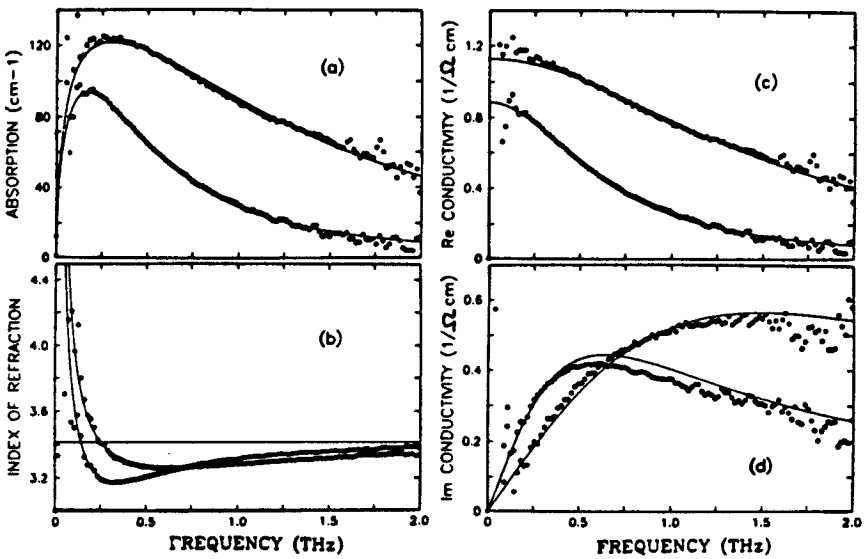

Fig.13 THz-TDS Results to 2 THz for 1.15-Ωcm, N-type (dots, lower curves) and 0.92-Ωcm, P-type (circles, upper curves) silicon. (a) Power absorption. (b) Index of refraction. (c) Real part of the electric conductivity. (d) Imaginary part of the electric conductivity.

in Fig. 13c and the imaginary part in Fig. 13d. The real part is strongly frequency dependent, dropping monotonically from its DC peak to a reduced value at the highest measured frequency of 2 THz. The extrapolated DC conductivities are 0.89 Ωcm for the P-type material and 1.13 Ωcm for the N-type, compared to the directly measured values of 0.92 Ωcm (P-type) and 1.15 Ωcm (N-type). The behavior of the imaginary part is completely different, increasing from zero at low frequencies, peaking at mid-range and then showing a gradual decline. The agreement with the Drude theory (solid line) is quite acceptable.

The two Drude parameters, the plasma angular frequency ω_p and the damping rate Γ, were determined within 5% accuracy from the fits to the data. For 0.92 Ωcm P-type silicon $\omega_p/2\pi =$ 1.75 THz and $\Gamma/2\pi =$ 1.51 THz, while for 1.15 Ωcm N-type silicon $\omega_p/2\pi$ = 1.01 THz and $\Gamma/2\pi$ = 0.64 THz. The measured damping rates and the known effective carrier masses, determine mobilities of 1680 cm^2/Vs for the electrons and 500 cm^2/Vs for the holes. The measured plasma frequencies and effective carrier masses determine the carrier densities of $1.4x10^{16}/cm^3$ for the P-type and $3.3x10^{15}/cm^3$ for the N-type silicon. Thus, these device-grade silicon wafers have been electrically characterized from low frequencies to 2 THz by THz-TDS.

D. THz Coherent Transients

An unusual and interesting observation by Harde et al (1991a,b) was that after excitation by a well-collimated beam of subpsec pulses of THz radiation, an N_2O vapor cell emitted a coherent THz pulse train extending to as long as 1 nsec. The N_2O molecule has a permanent electric dipole moment and a large number of strong rotational absorption lines with negligible Doppler broadening within the THz frequency range. The propagation of a 0.5 psec THz pulse through such a molecular vapor excites a multitude of rotational transitions in the impact approximation and causes the molecules to reradiate a free-induction-decay (FID) signal which decays because of relaxation, interference and propagation effects. Due to the experimental system's exceptionally high signal-to-noise ratio, the FID signal can be monitored to delay times as long as 1 nsec. Because the N_2O molecule has an almost constant frequency spacing between the rotational lines, a periodic rephasing and dephasing of the entire ensemble of the more than 50 excited transitions is observed. This situation contrasts to that of water vapor with a multitude of incommensurate resonance lines, studied earlier by THz time-domain spectroscopy by van Exter et al (1989b,c). Consequently, for N_2O vapor after the initial excitation pulse, the sample emits a series of uniformly spaced (39.8 psec) subpsec THz pulses whose amplitude decays with the coherent relaxation time T_2. From these observations T_2 can be directly determined, even under conditions when in the frequency domain the absorption lines would be completely overlapping. From the pulse repetition rate in the train the frequency separation between the rotational lines can be determined, and because of the exceptionally high time resolution of better than 0.5 psec, the anharmonicity in the linespacing can be detected as reshaping of the individual pulses in the train.

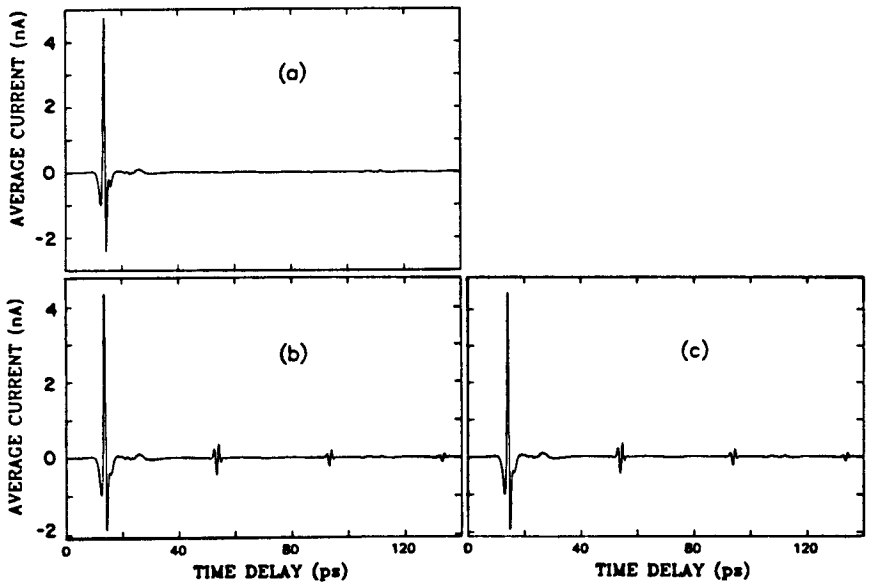

Fig.14 (a) Measured transmitted THz pulse to 140 psec without N_2O in the cell. (b) Measured THz pulse with 600 Torr N_2O vapor. (c) Calculated transmitted THz pulse through 38.7 cm of 600 Torr of N_2O vapor.

The measurements were performed on N_2O vapor within a 38.7 cm-long stainless steel cell having 2-cm-thick, 5-cm-diameter windows of 10 kΩ-cm silicon. For an evacuated cell the output pulse shown in Fig. 14a was obtained. When the cell is filled with 600 Torr of N_2O vapor, the output changes to that shown in Fig. 14b. Here, one sees the transmitted excitation pulse followed by 3 coherent transients emitted by the vapor. The amplitude of the first transient is 1/10 that of the excitation pulse.

Because the THz pulses are in the low-intensity limit of the Maxwell-Bloch equations, the interaction of the electric field with the sample is described in the frequency domain by simply introducing the absorption and dispersion of the vapor. The numerical calculation is performed as follows. The "input pulse" (Fig. 14a) is numerically Fourier analyzed. The resulting frequency components are multiplied by the amplitude absorption and phase change. The inverse numerical Fourier transform is performed giving the predicted output pulse . The fact that the "input pulse" includes reflections, some effects due to residual water vapor and system noise, yields the predicted

output pulses shown in Fig. 14c, that are remarkably similar to the actual observation. Every feature seen in the measurement of Fig. 14b, is reproduced in the calculation.

SUMMARY

A optoelectronic THz beam system has been described. The performance of the fastest version of this system is limited by the intrinsic time-response of the semiconductor. Driven by repetitive fsec laser pulses this system can generate and detect subpsec pulses of freely-propagating THz electromagnetic radiation with a signal to noise ratio of 1000:1 and a time resolution of 150 fsec. The importance of this system to THz time-domain-spectroscopy was illustrated by several examples of measurements. For these examples the high performance of the system was responsible for the THz-TDS results exceeding those obtained by the traditional methods of far-infrared (THz) spectroscopy.

ACKNOWLEDGEMENT

This work would not have been possible without the excellent masks and wafer fabrication by Hoi Chan. It has been my pleasure to have worked with the following outstanding scientists in my group for various lengths of time, while we developed the optoelectronic teraHz beam system described in this review and demonstrated its usefulness for THz time-domain-spectroscopy. The individuals are: Christof Fattinger (1987-1989), Martin van Exter (1988-1989), Søren R. Keiding (1989-1990), Hermann Harde (1990-6 months), Nir Katzenellenbogen (1990-, Stephen E. Ralph (1990-. It is my honor to be able to describe their many accomplishments.

REFERENCES

Auston D H 1983 Appl. Phys. Lett., Vol.43, 713.

Auston D H, Cheung K P and Smith P R 1984 Appl. Phys. Lett. Vol. 45, 284.

DeFonzo A P, Jarwala M and Lutz C R 1987a Appl. Phys. Lett., Vol.50, 1155; 1987b Vol.51, 212.

Doany F E, Grischkowsky D and Chi C C 1987 Appl. Phys. Lett. Vol. 50, 460.

Dykaar D R, Greene B I, Federici J F , Levi A F J, Pfeiffer L N and Kopf R F 1991 Appl. Phys. Lett., Vol.59, 262.

Fattinger Ch and Grischkowsky D 1988 Appl. Phys. Lett., Vol.53, 1480 ; 1989a Vol.54, 490; 1989b OSA Proc. on Psec. Elect. and Optoelect., T.C.L. Gerhard Sollner and D.M. Bloom, Eds. (Optical Society of America, Washington, DC), Vol.4.

Fattinger Ch and Grischkowsky D 1989c IEEE J. Quantum Electron., Vol.QE-25, 2608.

Gray D E 1982 "American Institute of Physics Handbook", Third Edition, McGraw-Hill Book Company (New York).

Greene B I, Federici J F, Dykaar D R, Jones R R and Bucksbaum P H 1991 Appl. Phys. Lett., Vol. 59, 893.

Grischkowsky D, Duling,III, I N, Chen J C, and Chi C-C 1987 Phys. Rev. Lett., Vol.59, 1663.

Grischkowsky D, Keiding S, van Exter M and Fattinger Ch 1990 J.Opt.Soc.Am.B, Vol.7, 2006. This paper contains a discussion and an extensive reference list describing the development of time-domain spectroscopy.

Grischkowsky D and Katzenellenbogen N 1991 OSA Proc. on Psec. Elect. and Optoelect., T.C.L. Gerhard Sollner, Jagdeep Shah, eds. (Optical Society of America, Washington, DC), Vol.9.

Harde H, Keiding S and Grischkowsky D 1991a Phys. Rev. Lett., Vol.66, 1834; Harde H and Grischkowsky D 1991b J. Opt. Soc. Am. B, Vol.8, 1642.

Heidemann R, Pfeiffer Th and Jager D 1983 Electronics Lett., Vol.19, 317.

Hu B B, Zhang X-C and Auston D H 1990 Appl. Phys. Lett., Vol.56, 506.

Johnson C, Low F J and Davidson A W 1980 Optical Engr., Vol. 19, 255.

Katzenellenbogen N and Grischkowsky D 1991 Appl. Phys. Lett., Vol. 58, 222.

Lesurf J C G 1990 "Millimetre-Wave Optics, Devices & Systems", (Adam Hilger, Bristol, England).

Loewenstein E V, Smith D R and Morgan R L 1973 Applied Optics, Vol. 12, 398.

Monteath G D 1973 "Applications of the Electromagnetic Reciprocity Principle", (Pergamon Press, Oxford).

Mourou G, Stancampiano C V, Antonetti A and Orszag A 1981 Appl. Phys. Lett., Vol.39, 295.

Pastol Y, Arjavalingam G, Halbout J-M and Kopcsay J V 1988 Electron. Lett., Vol. 24, 1318.

Pastol Y, Arjavalingam G, Halbout J-M 1990 Electron. Lett., Vol. 26, 133.

Ralph S E and Grischkowsky D 1991 Appl. Phys. Lett, Vol. 59, 1972.

Ralph S E and Grischkowsky D 1992 Appl. Phys. Lett., Vol. 60, 1070.

Russell E E and Bell E E 1967 J.Opt.Soc.Am. Vol.57, 543.

Smith P R, Auston D H, and Nuss M C 1988 IEEE J. Quantum Elect. Vol. 24, 255.

van Exter M, Fattinger Ch and Grischkowsky D 1989a Appl. Phys. Lett., Vol.55, 337.

van Exter M, Fattinger Ch and Grischkowsky D 1989b Optics Lett., Vol. 14, 1128; 1989c Laser Spectroscopy IX, Proceedings of the Ninth International Conference on Laser Spectroscopy, Bretton Woods, New Hampshire, June 18-23, 1989, edited by M.S. Feld, J.E. Thomas, and A. Mooradian, (Academic Press, Inc., San Diego).

van Exter M and Grischkowsky D 1990a Appl. Phys. Lett., Vol. 56, 1694; 1990b Phys. Rev. B15, Vol.41, 12,140.

van Exter M and Grischkowsky D 1990c IEEE Trans. Microwave Theory Tech., Vol.38, 1684.

Warren A C, Woodall J M, Freeouf J L, Grischkowsky D, McInturff D T, Melloch M R and Otsuka N, 1990 Appl. Phys. Lett., Vol.57, 1331.

Warren A C, Katzenellenbogen N, Grischkowsky D, Woodall J M, Melloch M R and Otsuka N, 1991 Appl. Phys. Lett., Vol.58, 1512.

Zhang X-C, Hu B B, Darrow J T, and Auston D H 1990 Appl. Phys. Lett., Vol.56, 1011.